Elaboration and characterisation of plasma sprayed alumina coatings on nickel with nickel oxide interlayer

Stéphane Valette, R. Bernardie, Joseph Absi, Pierre Lefort

Version of Record: https://www.sciencedirect.com/science/article/pii/S0257897221003339
Manuscript_80b1da0445b161833220b7577f3cf11c

Elaboration and Characterisation of Plasma Sprayed Alumina Coatings on Nickel with Nickel Oxide Interlayer

S. Valette*, R. Bernardie, J. Absi, P. Lefort.

University of Limoges, IRCER, UMR CNRS 7315, 12, rue Atlantis 87068 LIMOGES (France)

* Corresponding author

Abstract

A process implying the pre-oxidation of nickel substrates was proposed alternatively to the usual Atmospheric Plasma Spraying (APS) of alumina on sandblasted substrates. This process comprised two steps, the substrate pre-oxidation (instead of the sandblasting of the substrate) followed by APS. The pre-oxidation formed a thin layer of the NiO oxide, 0.7 – 3.5 µm thick, which entirely covered the nickel substrate. During APS, the deposit did not react with NiO due to the very high cooling rate of the alumina splats at the surface of the substrates. The characterisation of the interfacial zone showed the crystallographic continuity of the different lattices, from the nickel substrate (f.c.c.) to the NiO interlayer (f.c.c.) and to the monoclinic γ-Al_2O_3 coating. The NiO interlayer played the role of a buffer zone that adapted the crystal lattices of the three phases. The adhesion of the coatings was determined according to the ASTM C633 test modified by reducing the contact area substrate / coating, in order to quantify the adhesion of strongly-linked coatings. The coating adhesion reached 105 MPa for the pre-oxidized samples when NiO was 1.8 µm thick, instead of 48.5 MPa for the sandblasted samples and only 8 MPa for the simply polish nickel.

Keywords: nickel; alumina; adhesion; oxidation; plasma spraying

Highlights:

- The coating adhesion of Al_2O_3 on Ni is strongly improved by pre-oxidizing Ni
- The adhesions values are of 8 MPa for polished Ni and 48.5 MPa for sandblasted Ni
- The adhesion reaches 105 MPa for pre-oxidized Ni, then alumina-coated by APS
- At the interface, NiO is a buffer zone that adapts the Ni and γ-Al_2O_3 lattices

1. Introduction

In the field of Atmospheric Plasma Spraying (APS), it is commonly accepted that the ceramic coatings adhesion on metallic substrates strongly depends on surface condition of the substrates. Smooth surfaces or brittle surface oxides give poor adhesion while sandblasting provides good results [1] [2] [3]. In the case of alumina coatings on steels, the best results were obtained when the substrates underwent a controlled pre-oxidation [4]. This was due to the wüstite ($Fe_{1-x}O$) growth on the metal substrate by epitaxy, which provides the continuity of physical properties inside the interfacial zone, when going from the steel to the alumina coating through the interfacial zone [5].

This two steps process (substrate pre-oxidation and APS alumina coating) presents numerous advantages compared to the usual one (sandblasting and APS alumina coating), in particular because it can be used in the case of relatively complex substrates geometries and for thin samples, no silica grains remain at the interface substrate / coating, and it may provide better results in terms of adhesion. So, in the case of the coating by alumina, the adhesion was of 62 ± 2 MPa for a low carbon steel [6], reaching 73 MPa for 304L stainless steel [4], and even 82 ± 7 MPa [7] for C35 steel, while sandblasted steels did not give values higher than 50 MPa [2].

Now, this process has never been tested with nickel substrates, which might however present industrial interest in applications such as Waste-to-Energy plants [8,9]. A priori, nickel seemed to be a good candidate for this process insofar as its oxidation is considered producing the only oxide NiO, which grows by epitaxy on the metal [10], similarly as $Fe_{1-x}O$ on iron steels.

Hence, the aim of the present study was to achieve alumina coatings by APS on pre-oxidized nickel, in order to characterize the interfacial relationships and to test the coating adhesion. Indeed, the previous works devoted to systems giving good results in terms of adhesion have shown that there was a close link between

i) the nature (composition and microstructure) of the phases present at the interface substrate / coating;
ii) and the strength of the coating's adhesion.

The best conditions encountered were when the substrate and the oxide interlayer were in an epitaxy relationship and when, simultaneously, the oxide interlayer and the coating were in related by heteroepitaxy: in this case there was not any gap in the characteristics of the phases present in the interfacial zone [5]. Based on these considerations, the system Ni / NiO / Al_2O_3 seemed very favourable and, consequently, it had to be tested.

2. Materials and methods

2.1. Raw materials

2.1.1. Nickel

The substrates used were nickel plates, provided by Goodfellow ltd. The nickel was in the form of bars, 25 mm in diameter and 20 cm in length. Density and purity were equal respectively to 8.9 g/cm3 and 99.98% and the main impurities are given in Table 1. The XRD pattern of Fig. 1a shows that its crystal structure was face-centred cubic (f.c.c.), corresponding to the JCPDS file 04-007-0407.

The nickel microstructure observed in optical microscopy after polishing and chemical attack is given inFig.1b that shows a significant heterogeneity, with zones containing large polygonal grains, up to more than 50 µm (1), and zones with submicron grains and many narrow grain boundaries (2), but without any porosity.

The nickel bars were cut with a slow speed diamond saw in order to obtain small discs 25 mm in diameter and 5 mm thick. The samples were then either sandblasted with F 36 sand (corundum [-595, +420 µm]) for those which are not intended to be pre-oxidized, or manually polished on their two bases with silicon carbide abrasive papers (from 120 to 4000 mesh).

2.1.2. Alumina

The alumina powder used for the deposits was provided by Herman C. Stark, Germany (ref. AMPERITE 740.1, grain size [-45, +22 µm]). It was composed α-Al_2O_3 phase (corundum) as shown by the pattern of Fig. 2a (file JCPDS 46-1212), but it contained significant contents of oxides secondary phases, presented in Table 2, mainly Na_2O that can slightly lower its melting point. The powder presented the angular grain shapes characteristic of a molten powder crushed (see the SEM micrograph of Fig. 2b).

2.2. Formation of the NiO interlayer

The NiO interlayers (between the Ni substrates and the alumina coatings) were simply obtained by oxidizing the Ni samples at 940 °C according to eqn (1):

$$Ni + CO_2 = NiO + CO \quad (1)$$

A tubular furnace was used, crossed by flowing CO_2 (0.5 L min^{-1}, provider Air Liquide France, quality N27, purity of 99.7 vol. %). The choice of CO_2 instead of oxygen or air, which forms also the oxide NiO [11], was justified by the slower oxidation rate that allows better oxidation monitoring. The thickness of the oxide layers was easily adjusted by varying the oxidation times from 1.5 to 12 hours at 940°C, giving oxide layers thicknesses from 0.7 to 3.5 µm. After reaction, the nickel surface was entirely covered by a thin oxide

layer constituted of regular micron sized grains, well individualized (Fig. 3a) and composed only of NiO corresponding to the JCPDS file 04-012-6347 (see the XRD pattern of Fig. 3b). The presence of the Ni peaks in Fig. 3b was due to the weak thickness of the oxide layer (about 1.8 µm in this XRD analysis) that allowed seeing the response of the underlying substrate.

2.3. Plasma spraying

For plasma spraying, the torch Sulzer Metco PTF4 was used, following the usual procedure for the alumina deposits on metallic substrates, including a preheating step that favours the good spreading of the alumina splats [1,2] without allowing any reactivity, the temperature been limited at about 350 °C. During the APS, the samples were cooled by an air flow so that the samples temperature never exceeded 500 °C. The parameters used are given in Table 3.

2.4. Sample characterization

Microstructural investigations were carried out with a Scanning Electron Microscope (SEM) Philips XL 30, combined with an Energy Dispersive Spectroscopy (EDS). In order to improve SEM observations, samples were metallized, with 10 nm thick Pt coating, using AGAR SPUTTER COATER B7340 apparatus and conditions: 35 mm of work distance, Argon atmosphere (0.05 mbar) and sputter time of 45 s.

The phase identifications were performed with a Bruker D8 Advance diffractometer using the radiation $Cu_{K\alpha}$ (λ = 0.15418 nm), with back monochromator, and operating between 2θ angles of 20° and 80° with a step of 0.02 s and an exposure time of 0.9 s. The patterns were indexed with the software DIFFRAC+ containing the JCPDS data files.

The Transmission Electron Microscope (TEM) study was performed with a JEOL JEM-2100F instrument working at 200 kV and equipped with EDS device.

The adhesion of coatings was determined by following the tensile adhesion test (TAT) ASTM Standard C 633-13 and using a traction apparatus ADAMEL-LHOMARGY DY 26,

the samples being stuck on the dollies with the HTK ULTRA BOND 100® glue (HTK, Hamburg, Germany).

When the adhesion of coatings reached 50 MPa or more, which was what aimed, the usual ASTM TAT became inoperative because of ruptures inside the glue instead of at the substrate / coating interface. This question has been widely studied for other systems and many responses have been proposed [12, 13]. In the present study, the modified version of the test ASTM C 633 described in a recent paper [14] was used. This method had been applied to the case of alumina coatings on C35 steel and it is summarized by the scheme of Fig. 4. It consisted in painting the central part of the samples with a silver paint before coating, the effect of which being to reduce the contact area substrate / coating, while the contact area sample / dollies remained unchanged. The painted zone was a disk, achieved with a stencil placed in the middle of the sample: the larger the painted disk, the smaller the contact area substrate / coating, and the smaller the tensile strength required for get the coating unstuck. The silver paint was put after the pre-oxidation step, and before APS coating, so that it partially covered the oxide surface layer. It has been shown that the silver layer, about 8 – 10 µm thick, was not affected by the APS treatment.

3. Results and discussion

3.1. Preheating treatment

During the plasma spraying, the substrates are preheated for 90 s (see Table 3). As far as this treatment may impact the metal substrates, as seen in the case of ferrous substrates [15], the surface condition of nickel must be checked just after the preheating. The micrograph of Fig. 5a confirms that preheating caused the slight oxidation of nickel with the formation of small nuclei of NiO (a few tens of nm), which was verified by the XRD pattern of Fig. 5b.

For the pre-oxidized samples, no noticeable change in the nickel oxide grains was observed before preheating and after.

3.2. Spreading of the alumina splats

Fig.6 is a SEM micrograph representative of the alumina splats spread on the surface of the nickel substrates covered by NiO. The molten alumina produced splats that splashed on the oxide surface. This illustrates the good wetting of alumina on the nickel oxide which constitutes a point favourable for obtaining the good adhesion of the coating [1].

3.3. Crystallographic and morphological characterization of the Ni / NiO / Al_2O_3 multilayer

Fig. 7 presents a cross section of the interfacial zone between the nickel substrate and the alumina coating, with the NiO interlayer. The oxide layer, where the micron sized NiO crystals are clearly visible, has an uneven thickness of about 1.8 µm, with irregular upper and lower interfaces but without cracks and without pores inside the different phases, showing that they were not affected by the cutting and the polishing necessary for the sample preparation before observation. All this constitute favourable conditions for a good bonding of the materials.

3.3.1 Coating characterization

The alumina coating presented the same characteristics as already observed in the case of other similar deposit [4, 16]. The coating fracture of Fig. 8a shows that, inside the coating, the alumina grains were angular and about 5 to 10 µm large, while the surface (Fig.8b) was composed of molten or semi-molten particles, with open porosity and numerous micro-cracks. The cross-section of Fig.8c reveals the porous microstructure of the deposit, with an homogeneous distribution of the pores, approximately 2 µm in size.

The X-ray diffraction pattern of the coating surface, presented in Fig.8d, identified mainly the metastable γ-alumina phase (JCPDS file 01-077-0396) with the intense (400) and (440) peaks, well defined and relatively narrow. The lower amplitude and the widening of the peaks (222), (311) and (511), often observed in such APS deposits, is generally attributed to the presence of gaps in the cation lattice of aluminium ions [17, 18]. The α alumina phase that corresponds to the initial powder (JCPDS file 00-010-0173), thermodynamically stable below

2300 K [19], is present in lower quantity, such as the transition δ alumina (JCPDS file 00-046-1131), which results from the solid-phase transformation of γ-alumina due to the impact of liquid particles on solid surfaces [20, 21].

The transmission electron microscopy (TEM) analysis carried out inside the coating identified the γ-alumina phase with its columnar structure visible in Fig.9a. The corresponding electron diffraction pattern of Fig.9b confirms the only presence of the γ alumina spots, with diffuse, oriented and elongated satellites in the directions [100]. These satellites are close to the diffraction spots of the cationic sub-lattice (200), (220) and they were attributed to the more or less ordered arrangement of cations and to gaps in the cationic sub-lattice [17, 18, 21].

3.3.2 Characterization of the interfacial zone

TEM observations of the interfacial zone were carried out on a nickel sample oxidized during 2 hours at 940 °C in flowing CO_2 with an average thickness of 1.0 µm. Fig. 10 gives the overview of the interfacial zone comprising the substrate (nickel), the intermediate layer of nickel oxide and the alumina coating. The clear phase visible in the middle of the alumina is the remaining of the glue used during the sample ionic thinning. The two nickel / oxide and oxide / alumina interfaces are clearly defined, without any crack. The oxide layer consists in a stack of small grains (0.5 – 1 µm) that is consistent with the SEM observations of Fig. 3a.

The TEM image of Fig.11a details the NiO / Al_2O_3 interface with the SAED pattern corresponding (Fig. 11b), which present a splitting of the diffraction spots, indicating the presence of two phases having similar structures and lattice parameters. Moreover, the zone axis [011] is common for both oxides (see Fig.11c) that is characteristic of the homoaxial heteroepitaxy of the two phases, which would not be possible for lattice parameters very different, as 0.4173 nm for f.c.c. NiO (JCPDS file 04-012-6347) and, for γ-Al_2O_3, a = 0.796 nm and b = 0.781 nm (spinel structure, with a tetragonal distortion) [22]. Now, the γ-Al_2O_3 structure is currently no more considered as distorted spinel but as monoclinic, with lattice

parameters a = 0.5587 nm, b = 0.8413 nm and c = 0.8068 nm [23]. Hence, the continuity of the oxygen lattices is possible between both phases NiO and γ-Al_2O_3. Indeed, when cooling, the alumina splats may crystallise easily by taking up a crystal structure close to that of the underlying NiO: this induces only little adaptation of its anion network. Fig.12 illustrates this adaptation with a 2D representation according to the (110) plane. According to the *b* direction, the distance between the O^{2-} ions is of 0.42065 nm in alumina (0.8413/2) and 0.4173 nm in NiO, i.e. only 0.00335 nm less, which represents only 0.8 %. Seen the relative closeness of the lattice parameters b (0.8413 nm) and c (0.8068 nm) of γ-Al_2O_3, the representation would be similar according to the plane (101): this time, the distance between the O^{2-} ions is 0.0139 nm smaller in the Al_2O_3 lattice than in the NiO one (- 3.4 %) according to the *c* direction. However, it should be noticed that this mode of adaptation of the lattices does not exclude the possibility of some dislocations in the *a* direction [24, 25].

In short, the closeness of the anion distances in the *b* and *c* directions allows the crystallographic continuity by heteroepitaxy of the lattices NiO and γ-Al_2O_3 in the interfacial zone. The succession of phases {Ni / NiO / γ-Al_2O_3 / α-Al_2O_3 and δ-Al_2O_3} constitutes a kind of buffer zone between the nickel and the alumina coating, which brings the physical and crystallographic continuity between both materials: (Ni / NiO: epitaxy; NiO / γ-Al_2O_3: heteroepitaxy; γ-Al_2O_3 / α-Al_2O_3 and δ-Al_2O_3: mix of allotropes γ, monoclinic, α, hexagonal, and δ, orthorhombic).

3.4 Adhesion of the coatings

3.4.1 Measurements with the conventional protocol ASTM C633

The tensile tests were carried out following the conventional protocol ASTM C633-13 on three types of substrates coated with alumina:

i) for the batch 1, nickel was simply polished (up to the SiC paper of 4000 mesh);
ii) the batch 2 was constituted of the sandblasted substrates that is the usual process of APS deposition [4]

iii) and the batch 3 comprised the substrates pre-oxidized at 940 °C in flowing CO_2 with different oxide thicknesses: 0.7 ± 0.15, 1.5 ± 0.2, 2.5 ± 0.2 and 3, 9 ± 0.25 µm.

The batches 1 and 2 were tested only in order to determine the improvement brought by the pre-oxidation process compared to the usual APS methods, the batch 3 having undergone neither polishing nor sandblasting.

For the batches 1 and 2, 5 samples were tested, and for the batch 3, 5 samples were tested for each oxide thickness. The results of the adhesion tests are summarized in Table 4, the uncertainties corresponding to the standard deviations.

For the polished samples, the breaking load is low, confirming the poor adhesion of the APS ceramic coatings on polished metallic substrates [2].

The effect of the sandblasting was significant since the adhesion reached around 50 MPa. This value is close to that observed for alumina deposits on other sandblasted substrates, this result being attributed to the clasp of the molten splats around the asperities created by the sandblasting at the substrates surface [2]. In this case, the coating adhesion only depends on the surface condition of the substrate, and not on the substrate nature: logically, the adhesion values are comparable whatever the substrate nature.

Besides, this method constitutes the usual industrial initial treatment for APS, but the rupture remains adhesive, and it occurs always at the coating / substrate interface.

At the opposite, for the pre-oxidized and coated substrates, the rupture never occurred at this interface but at the junction with the glue (interfaces alumina / glue or dollies / glue). This made impossible the quantification of the adhesion of the deposits, but this result proved that the adhesion of alumina deposits was higher with the pre-oxidized nickel substrates than with the sandblasted substrates, whatever the NiO thickness. Hence, the adhesion determination required the tests ASTM C 633 modified for strongly bonded coatings described before in § 2.4.

3.4.2 Measurements on pre-oxidized and coated samples with the modified protocol ASTM C633

The measurements were carried out on substrates with two thicknesses of pre-oxidized layers, 1.8 ± 0.4 µm and 3.5 ± 0.4 µm, respectively obtained after 5 and 12 hours oxidation at 940°C in flowing CO_2. The areas covered by the silver paint (see Fig. 4) were discs of 4, 8, 12, 16 and 20 mm in diameter. For each defect diameter, 5 samples were tested. The results are given in Fig.13, each point corresponding to the average of the measurements made on the batch of the 5 samples, and the error bar represents the standard deviation of the measurements.

For the silver defect diameters lower than 16 mm, fractures always occurred at the junction between the glue and the dollies or at the junction between the glue and the sample (no cohesive rupture of the glue was observed, the cohesion of which being higher than 100 MPa). For the largest defect sizes, the ruptures occurred inside the sample between the substrate and the coating, and the applied force at breaking F was proportional to the contact area S (sample / coating, excluding the defect area) according to eqn (2):

$$F = \sigma_r \times S \qquad (2)$$

The proportionality coefficient σ_r is the adhesion of the coating [14].

The so determined adhesion values were 105 ± 10 MPa and 77 ± 8 MPa for the oxide thicknesses of 1.8 and 3.5 µm, respectively. These results confirmed that the coating adhesion was significantly higher for the pre-oxidized samples than for the sandblasted ones.

Fig.14 gathers the results obtained on the samples, pre-oxidized or not, as a function of the thickness of the nickel layer. It is likely that an optimal oxide thickness exists, either less than 1.8 µm, or between 1.8 and 3.5 µm, but this would require extra tests with other oxide thicknesses for more precision.

3.4.3 Characterisation of the interfacial zone after breaking

After the tensile tests, the broken pieces were analysed in order to characterize the interfacial zone for the three kinds of substrates (polished, sandblasted and pre-oxidized). In each case, the two surfaces created by the breaking were observed and analysed by XRD: that on the deposition side (alumina) and that on the substrate side (nickel).

3.4.3.1 Polished samples

After breaking, the substrate surface S_S presented exactly the same morphology as seen in Fig.5, and XRD identified always the peaks of Ni with the small amounts of NiO that resulted from the thermal treatment before coating. This confirms that, even in the case of polish samples, there was always a thin NiO interlayer between the substrate and the coating. XRD pattern of the alumina surface S_D (previously in contact with Ni) reported in Fig. 15, identifies the presence of traces of NiO together with the peaks of the different alumina phases characteristic of the coating, already seen in. Fig 8.

The rupture occurred at the level of the NiO nuclei, as oxide traces remained hitched as well with the nickel as with the alumina deposit. Not any phase resulting from a possible reaction between NiO and Al_2O_3 was identified; besides, such phases have never been observed in similar systems and this is considered as due to the too high cooling rate of the splats at the surface of the substrates (10^7-10^8 $K.s^{-1}$ [1][2]).

Hence, the poor adhesion of the coating in the case of polish substrates was attributed to the brittleness of the junctions both between the substrate and the oxide nuclei and between the oxide nuclei and the deposit, which means, in particular, that the NiO nuclei were not solidly linked with the metal.

3.4.3.2 Sandblasted samples

The alumina surface S_D, previously in contact with NiO, observed in Fig. 16a contained traces of nickel oxide as shown by the EDS analysis of Fig.16b and by the XRD pattern of Fig. 16c. The presence of nickel oxide resulted from the wrenching of the substrate asperities clenched by the alumina splats during APS.

The substrate surface S_s, is presented in Fig. 17 with its EDS analysis showing that it was only composed of nickel, i.e. that the oxide formed during the preheating completely moved with alumina when breaking. This confirms, here again, that the NiO nuclei formed during the preheating treatment were not strongly fixed the substrate. The SEM micrograph of Fig. 17 shows also some inclusions identified by EDS as alumina that remained in the holes of the sandblasted substrate.

Hence, in the case of sandblasted samples, the coating adhesion was due to the substrate asperities clutched by the alumina splats as already seen in other systems [1][2].

3.4.3.1 Pre-oxidized substrates

The analysed samples were the substrates pre-oxidized at 940°C in flowing CO_2, with the NiO layer 1.8 ± 0.4 µm thick, then partially covered by the silver paint (disk 16 mm in diameter), then alumina coated, and finally broken by the TAT.

The alumina surface S_D, previously in contact with NiO, observed in Fig. 18, was partially covered by small NiO grains, the alumina grains being only visible in places (see the corresponding EDS analyses) representing about 30 % of the overall surface. The presence of platinum in the EDS spectra came from the metallization made for improving the SEM observations.

When examining the substrate surface (Fig. 19) the presence of the small NiO grains was again identified, but some alumina grains were also present (see the EDS analyses), and they covered again about 30 % of the surface. These analyses proved that, for the pre-oxidized samples, the rupture mainly occurred inside the nickel oxide (cohesive rupture) since this phase was found as the main constituent of both surfaces created by the breaking. This kind of cohesive failure implies the propagation of the micro-cracks between the NiO grains. It can be noticed that It can also be observed that NiO was strongly linked with the Ni substrate when the NiO layer was thick, which was not the case with the small surface nuclei of NiO (for the

polish or the sandblasted samples). This means that the anchoring of the NiO grains necessitated they reached a minimum size.

Nevertheless, the presence of some alumina grains on both surfaces implied that the rupture also occurred, for a minor part, at the level of the first alumina splats, which was the sign of a cohesive failure, occurring inside the alumina coating. The excellent complementarity of the surfaces covered by NiO in the coating side, with those covered by Al_2O_3 showed that the failure occurred either inside NiO, or inside Al_2O_3 but seldom at the interface itself, at the opposite of what observed in the case of polish or sandblasted samples. This meant that the adhesive rupture was minority, due to the solidity of the bonding.

4. Conclusion

The present study was based on the starting hypothesis that the system {Ni / NiO / Al_2O_3} could be allow obtaining APS alumina coatings strongly bonded to the Ni substrates, by analogy with the system {Fe / $Fe_{1-x}O$ / Al_2O_3} where the excellent adhesion of the coating had been justified by "crystallographic bonding" [5, 6]. Effectively, the obtained results were favourable:

- The adhesion of the APS alumina coatings on pre-oxidized nickel reached 105 MPa, value by far higher than that obtained by APS on sandblasted substrates, which was of 48.5 MPa, itself higher than that obtained with polished samples (8 MPa);
- The tensile adhesion tests showed that the ruptures occurred mainly inside the NiO layer formed during the pre-oxidation step: NiO is the weak link of the assembly {Ni / NiO / Al_2O_3};
- The thickness of the NiO layer is a significant parameter that could be optimized. The best results could be included in the range [0 – 1.8 µm]. Moreover, perhaps that the NiO microstructure could be also optimized, since

the cracks propagated between the small grains of NiO, and smaller grains could provide better results;

- The origin of the strength of the bonding between alumina and pre-oxidized nickel was identified. This was due to two factors: the epitaxy relationship between Ni and the oxide NiO [26, 27], and the homoaxial heteroepitaxy between the f.c.c. NiO and the monoclinic γ- Al_2O_3. Globally, the NiO interlayer constituted a buffer zone that allowed adapting the crystallographic structure of Ni with that of Al_2O_3: without the NiO interlayer, not any relationship is possible between Ni and Al_2O_3, neither chemical nor crystallographic.

Clearly, the strength of the bonding between pre-oxidized nickel substrates and alumina coatings was due to specificities in the system {Ni / NiO / Al_2O_3}, which is analogous to the system {Fe / $Fe_{1-x}O$ / Al_2O_3}, but the APS process with the pre-oxidation of the metal substrate cannot be enforced successfully for any couple metal substrate / ceramic coating.

References

[1] P. Fauchais, M. Vardelle, S. Goutier, Atmospheric Plasma Spraying evolution since the sixties through modelling, measurements and sensors, Plasma Chem. Plasma Process. 37 (2017) 601-626.

[2] M. Mellali, P. Fauchais, A. Grimaud, Influence of substrate roughness and temperature on the adhesion / cohesion of alumina coatings, Surf. Coat. Technol. 81 (1996) 275-286.

[3] S. Leigh, C. Berndt, A test for coating adhesion on flat substrates - a technical note, J. Therm. Spray Technol. 3 (1994) 184-190.

[4] F. Goutier, S. Valette, M. Vardelle, P. Lefort, Alumina plasma spraying on 304L stainless steel: Role of a wüstite interlayer, J. Eur. Ceram. Soc. 31 (2011) 1685-1694.

[5] S. Valette, G. Trolliard, A. Denoirjean, P. Lefort, Iron/wüstite/magnetite/alumina relationships in plasma coated steel: A TEM study, Solid State Ionics 178 (2007) 429-437.

[6] S. Valette, A. Denoirjean, P. Lefort, Plasma sprayed steel: Adhesion of an alumina film via a wüstite interlayer, Surf. Coat. Technol. 202 (2008) 2603-2611.

[7] R. Bernardie, S. Valette, J. Absi, P. Lefort, Mechanical characterization of alumina coatings on C35 steel, Surf. Coat. Technol. 276 (2015) 677-685.

[8] A. Phongphiphat, C. Ryu, Y.B. Yang, K.N. Finney, A. Leyland, V.N. Sharifi, J. Swithenbank, Investigation into high-temperature corrosion in a large-scale municipal waste-to-energy plant, Corr. Sci., 52 (2010) 3861–3874.

[9] A. Phongphiphat, C. Ryu, K.N. Finney, V.N. Sharifi, J. Swithenbank, Ash deposit characterisation in a large-scale municipal waste-to-energy incineration plant, Journal of Hazardous Materials, 186 (2011) 218-226.

[10] N. Vallino, L. Lahoche, V. L. Lorman, S. B. Rochal, J. M. Roelandt, Influence of epitaxy and ordering on the mechanical behaviour of an oxide layer on a metallic substrate, Surf. Coat. Technol., 108-109 (1998) 442-448.

[11] R. Peraldi, D. Monceau, S. Jean, B. Pieraggi, High temperature oxidation of high purity nickel: Oxide scale morphology and growth kinetics, Mater. High Temp., 20 (2003) 649-655.

[12] C.C. Berndt, Tensile adhesion testing methodology for thermally sprayed coatings, J. Mater. Eng., 12-2 (1990) 151–158.

[13] A.S.M. Ang, C.C. Berndt, A review of testing methods for thermal spray coatings, Int. Mater. Rev., 59-4 (2014) 179–223.

[14] R. Bernardie, R. Berkouch, S. Valette, J. Absi, P. Lefort, Experimental and numerical study of a modified ASTM C633 adhesion test for strongly-bonded coatings, J. Mech. Sci. Technol., 31 (2017) 3241-3247.

[15] J. Pech, B. Hannoyer, O. Lagnoux, A. Denoirjean, P. Fauchais, Influence of preheating parameters on the plasma-jet oxidation of a low-carbon steel, High Temp. Mater. Proc., 15 (2011) 51-60.

[16] L. Bianchi, A. Grimaud, F. Blein, P. Lucchese and P. Fauchais, Comparison of plasma-sprayed alumina coatings by RF and DC plasma spraying, J. Therm. Spray Technol., 4 (1995) 59-66.

[17] Y. Repelin, E. Husson, Etudes structurales d'alumines de transition. I-Alumines gamma et delta, Mater. Res. Bull., 25 (1990) 611-621.

[18] I. Levin, D. Brandon, Metastable alumina polymorphs: crystal structures and transition sequences, J. Am. Ceram. Soc., 81 (1998) 1995-2012.

[19] I. BARIN, Thermochemical data of pure substances, 2nd ed., VCH, 1993.

[20] S. Kuroda, T. Dendo, S. Kitahara, Quenching stress in plasma Sprayed Coating and its Correlation with the Deposit Microstructure, J. Therm. Spray Technol., 4 (1995) 75-84.

[21] J. M. Guilemany, J. Nutting, M. J. Dougan, A Transmission Electron Microscopy Study of the Microstructures Present in Alumina Coatings Produced by Plasma Spraying, J. Therm. Spray Technol., 6 (1997) 425-429.

[22] S.J. Wilson, The dehydration of Boehmite γ-AlOOH to γ-alumina, J. Solid State Chem., 30 (1979) 247-255.

[23] X. Krokidis, P. Raybuaud, A. E. Gobichon, B. Rebours, P. Euzen, H. Touloat, Theoretical study of the dehydration process of boehmite to γ-alumina, J. Phys. Chem. B, 105 (2001) 5121-5130.

[24] B. Pieraggi, R. Rapp, Stress generation and vacancy annihilation during scale growth limited by cation-vacancy diffusion, Acta Metall., 36 (1988) 1281-1289.

[25] B. Pieraggi, R. Rapp, J. Hirth, Role of interface structure and interfacial defects in oxide scale growth, Oxid. Met., 44 (1995) 63-79.

[26] M. Leseur, B. Pieraggi, Structure of metal-oxide interfaces, J. Phys., 46, C4 (1985) 135-140.

[27] H.T. Sawhill, L.W. Hobbs, Structure and energy of Ni/NiO interfaces, J. Phys., 46, C4 (1985) 117-122.

Tables

Table 1
Nickel main impurities

Elements	Ppm
C	70
Cu	10
Fe	10
Mg	10
Mn	10
Ti	10
Co	8
Cr	8
Si	8

Table 2
Alumina powder composition

Phases	wt.%
Al_2O_3	99.55
Fe_2O_3	0.05
Na_2O	0.30
SiO_2	0.1

Table 3

Plasma spraying parameters used for alumina coatings

Plasma gas mixture	Ar/H_2
Plasma gas flow rates	(slm) 45 (Ar)/15 (H_2)
Arc current/voltage	600 A/62 V
Nozzle	7 mm
Spray distance	100 mm
Powder mass flow rate	20 g/min
Rotational velocity	180 rpm
Oscillation linear velocity	24 mm/s
Preheating temperature/duration	about 350 °C/90 s
APS duration/ coating thickness	240 s/ about 260 µm

Table 4

Results of the tensile tests of the coatings according to the test ASTM C633

Substrate	Rupture location	Adhesion (MPa)
Polished	At the interface Ni / Al_2O_3	8.0 ± 4
Sandblasted	At the interface Ni / Al_2O_3	48.5 ± 4
Pre-oxidized (e_{NiO} = 0.7 ± 0.15 µm)	At the junction with the glue	55 ± 2
Pre-oxidized (e_{NiO} = 1.5 ± 0.2 µm)	At the junction with the glue	51 ± 3
Pre-oxidized (e_{NiO} = 2.5 ± 0.2 µm)	At the junction with the glue	49.5 ± 4
Pre-oxidized (e_{NiO} = 3.9 ± 0.25 µm)	At the junction with the glue	49 ± 3

List of figure captions

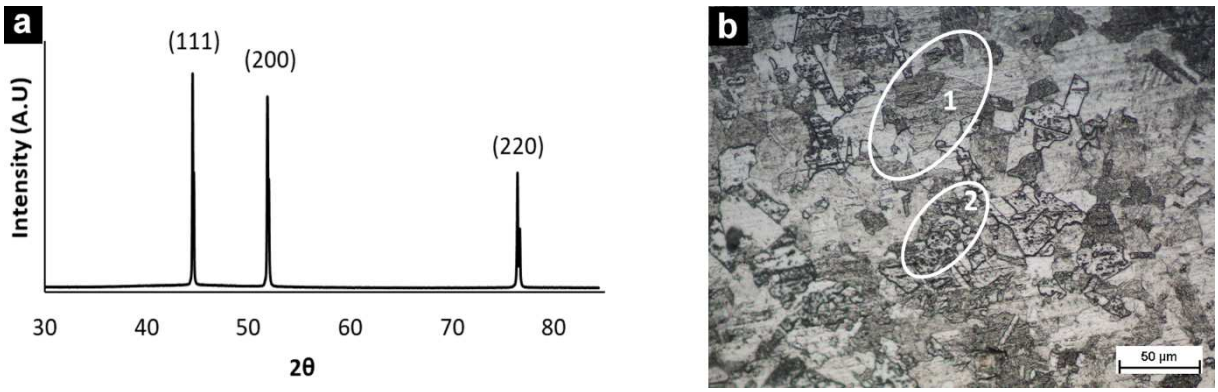

Figure 1

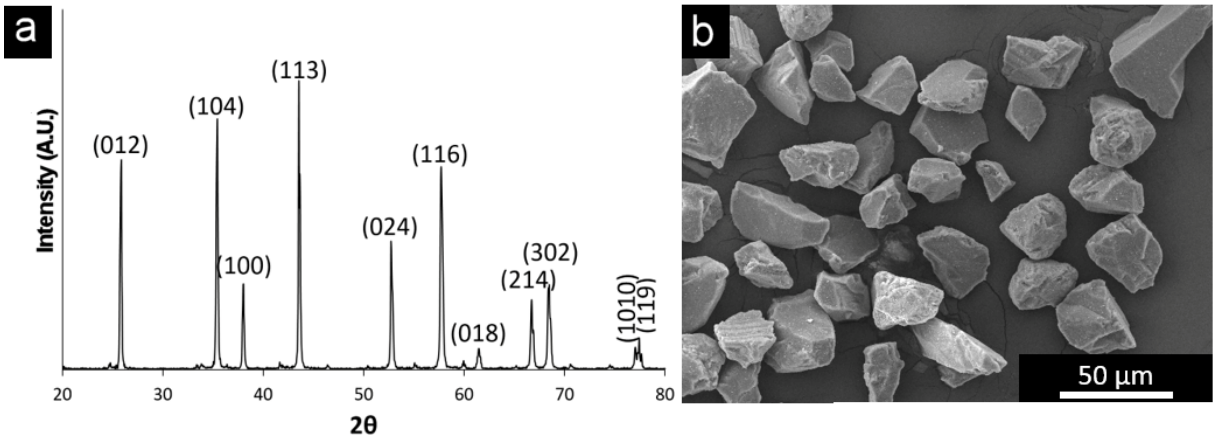
a
Intensity (A.U.)
(012)
(104)
(100)
(113)
(024)
(116)
(018)
(214)
(302)
(1010)
(119)
20
30
40
50
60
70
80
2θ
b
50 µm

Figure 2

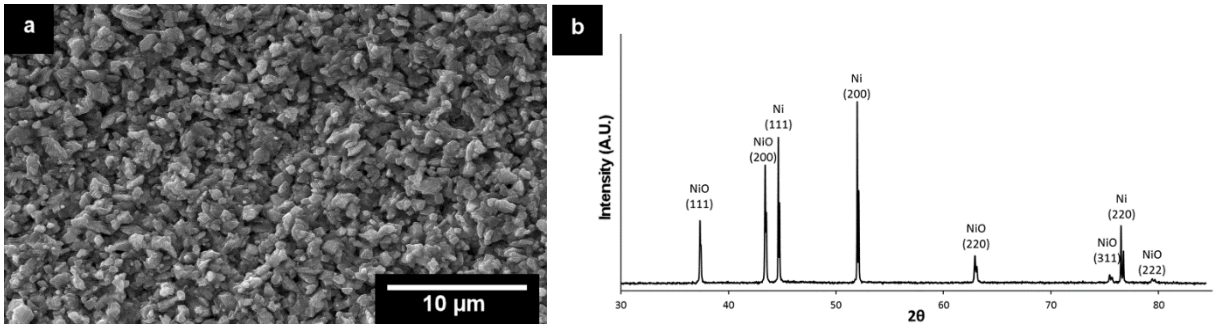
a
10 µm
b
Intensity (A.U.)
NiO
(111)
Ni
(111)
NiO
(200)
Ni
(200)
NiO
(220)
Ni
(220)
NiO
(311)
NiO
(222)
30
40
50
60
70
80
2θ

Figure 3

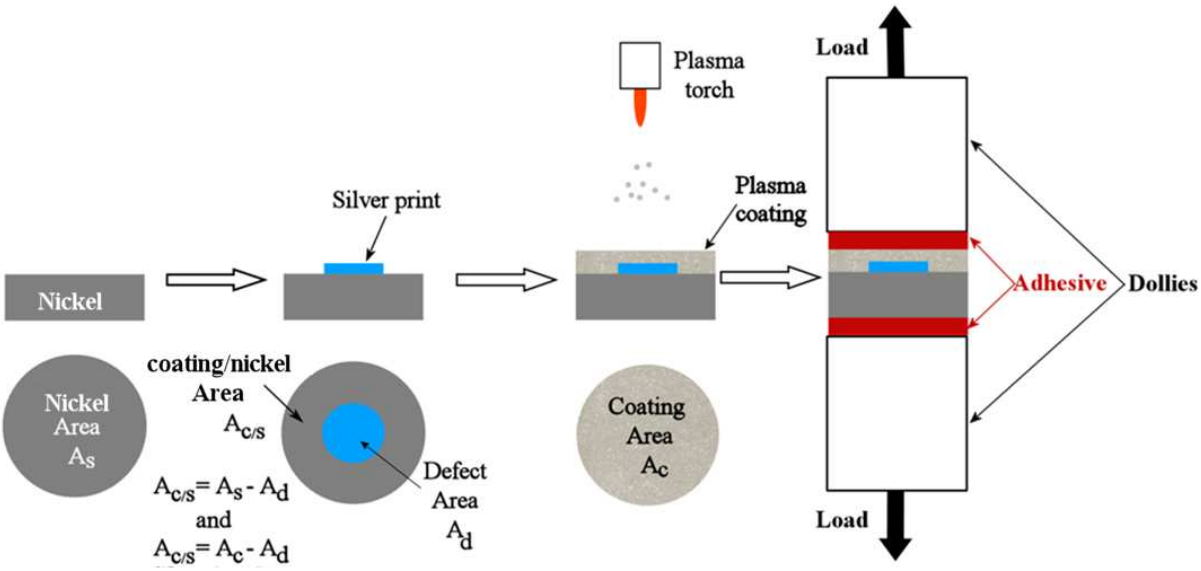
Plasma
torch
Load
Silver print
Plasma
coating
Nickel
Adhesive
Dollies
Nickel
Area
A_s
coating/nickel
Area
$A_{c/s}$
$A_{c/s} = A_s - A_d$
and
$A_{c/s} = A_c - A_d$
Defect
Area
A_d
Coating
Area
A_c
Load

Figure 4

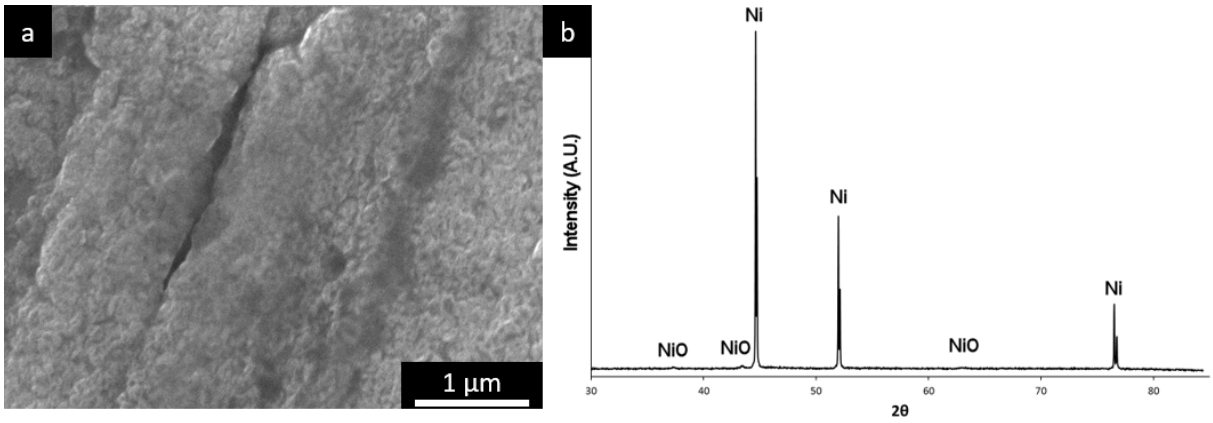

Figure 5

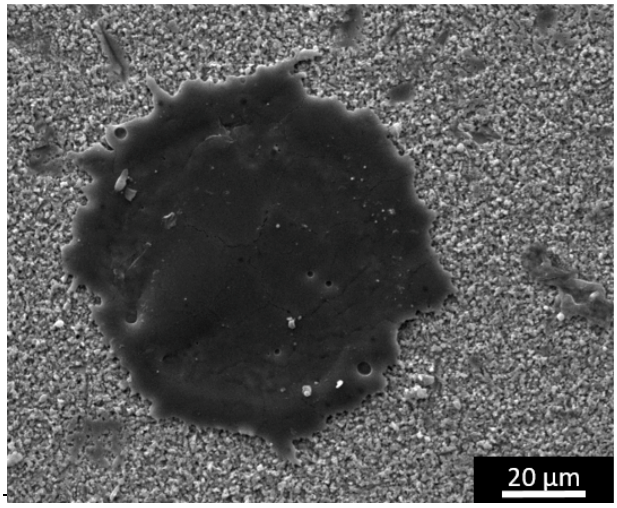

Figure 6

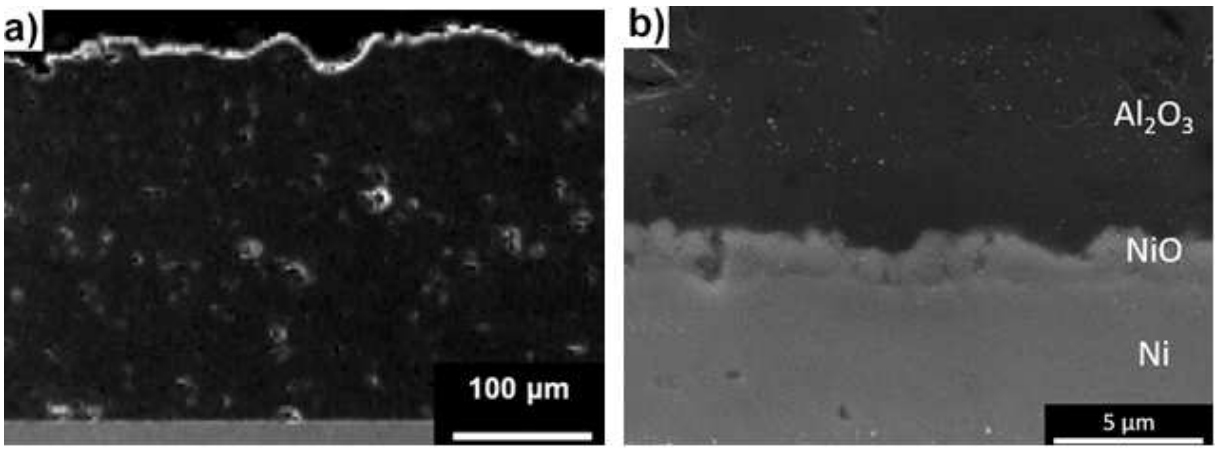

Figure 7

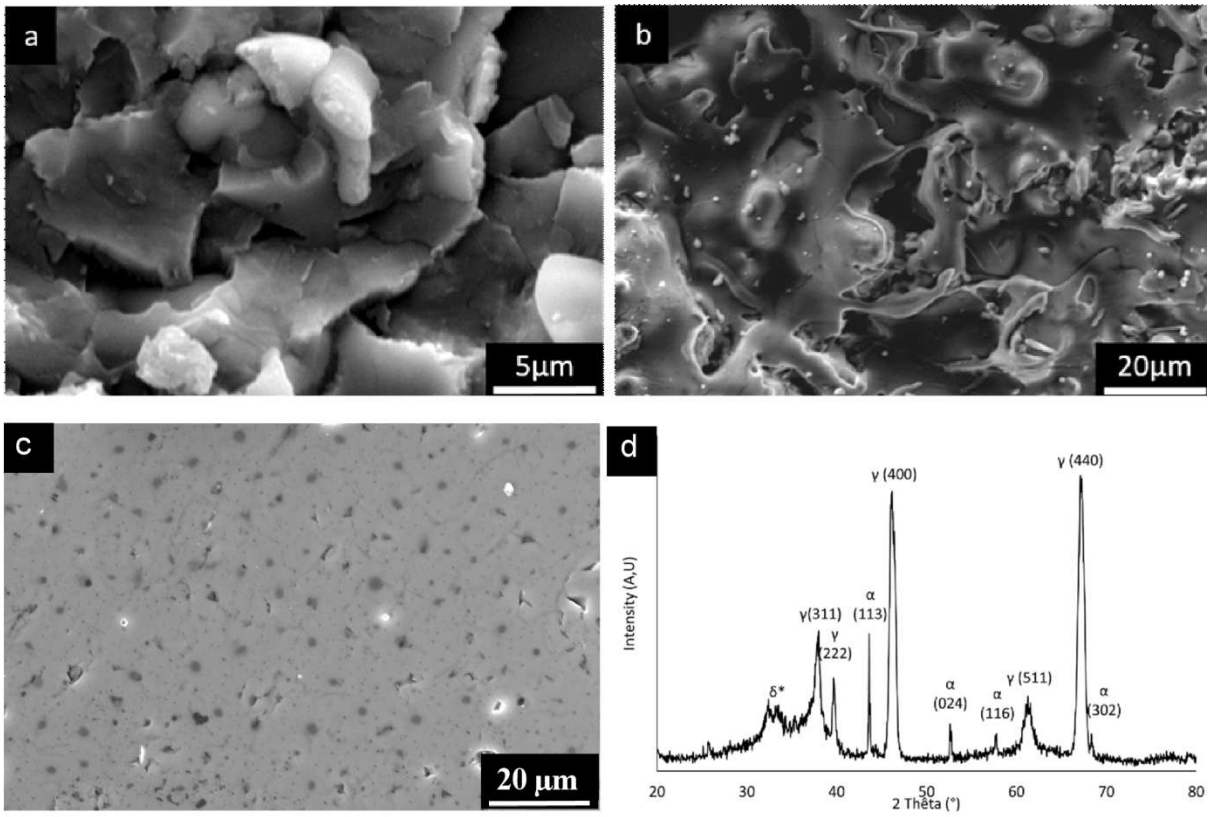
a
5µm
b
20µm
c
20 µm
d
γ (400)
γ (440)
γ(311)
α (113)
γ (222)
δ*
α (024)
α (116)
γ (511)
α (302)
Intensity (A.U)
20
30
40
50
60
70
80
2 Theta (°)

Figure 8

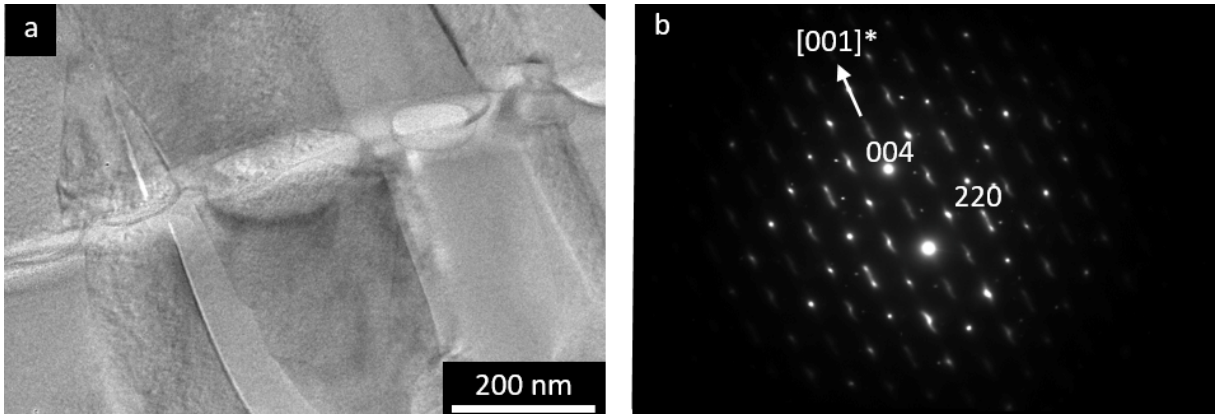

Figure 9

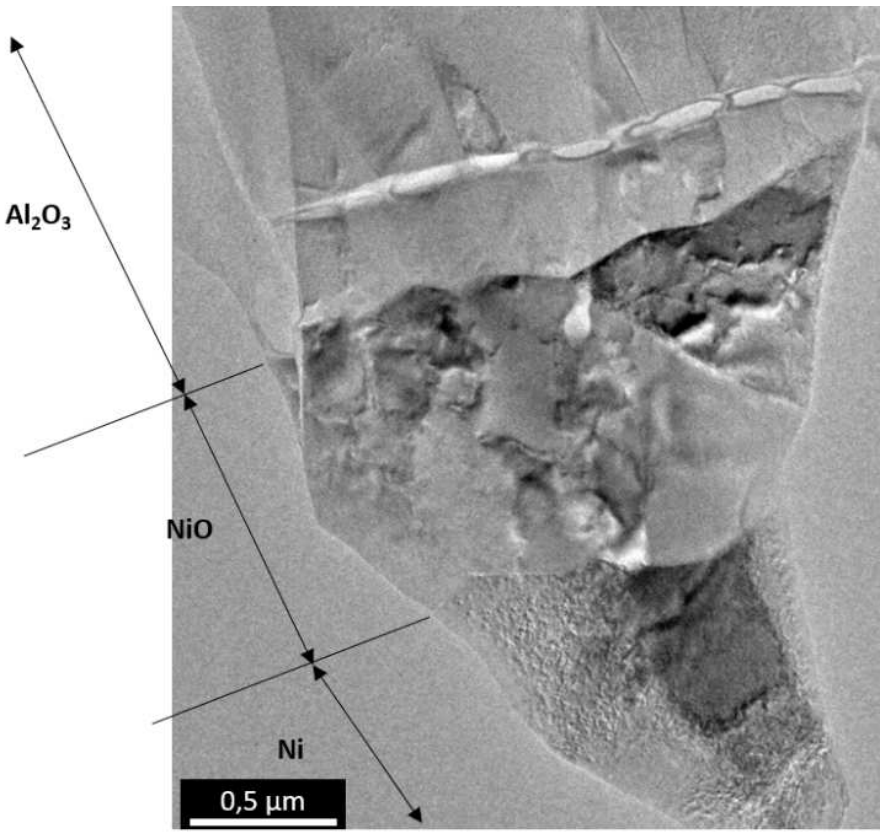

Figure 10

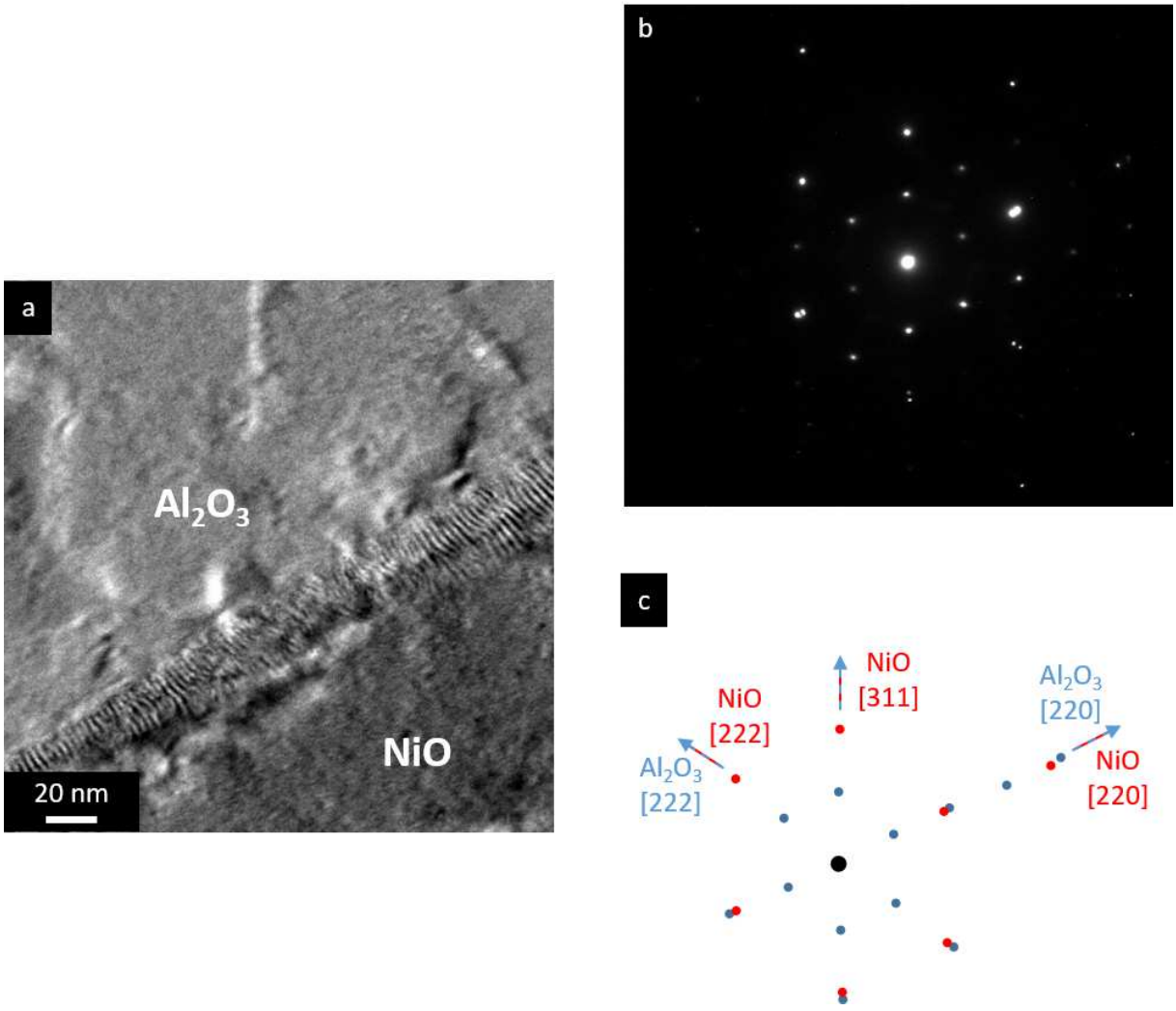

Figure 11

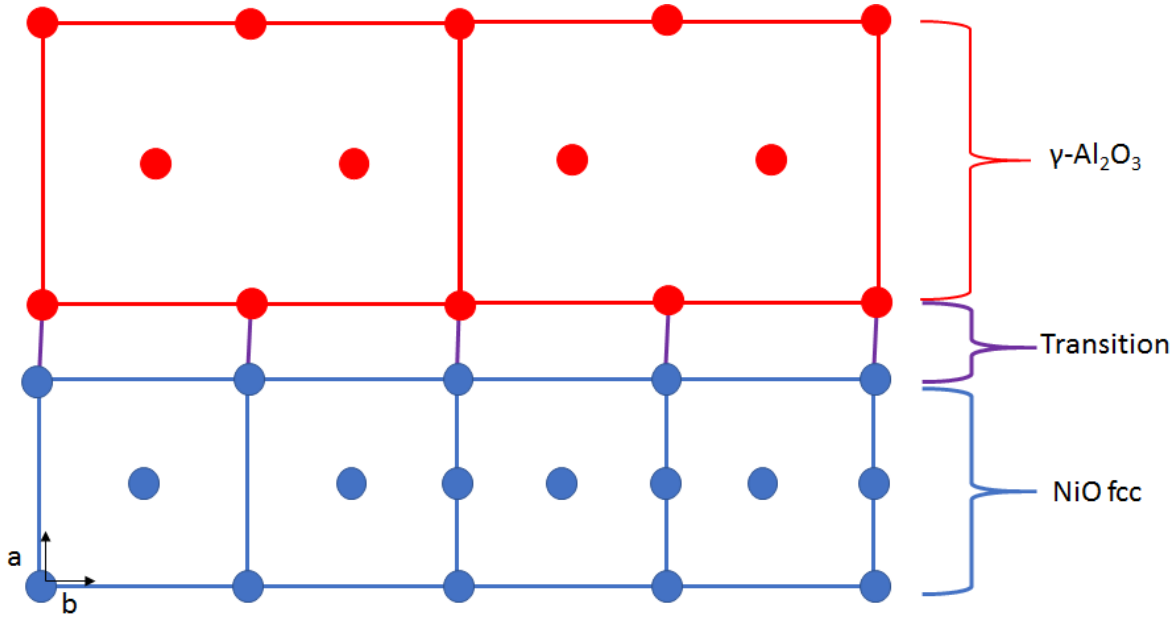

Figure 12

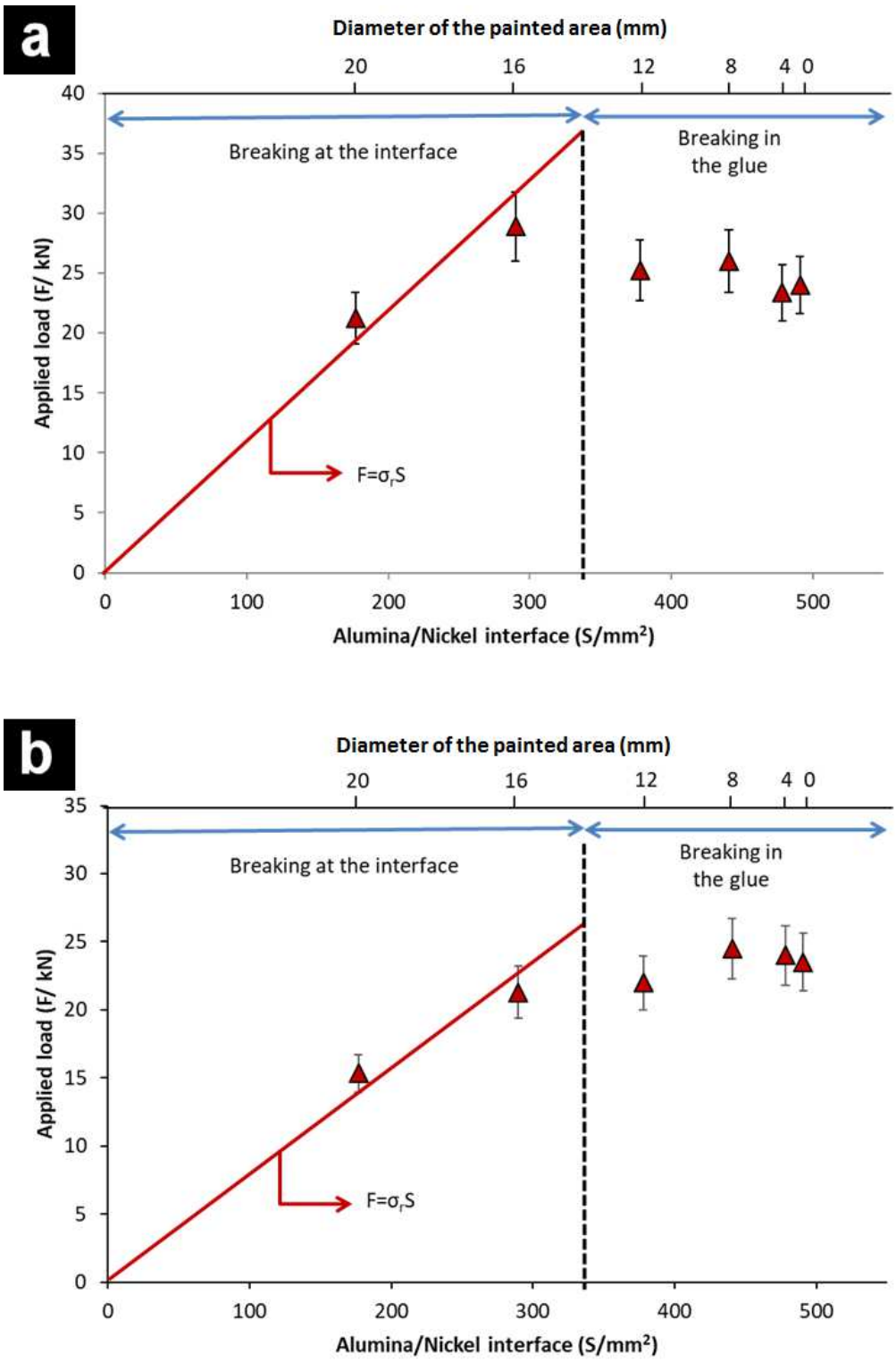
a
Diameter of the painted area (mm)
20
16
12
8
4
0
Breaking at the interface
Breaking in the glue
Applied load (F/ kN)
F=σrS
Alumina/Nickel interface (S/mm²)
b
Diameter of the painted area (mm)
Breaking at the interface
Breaking in the glue
Applied load (F/ kN)
F=σrS
Alumina/Nickel interface (S/mm²)

Figure 13

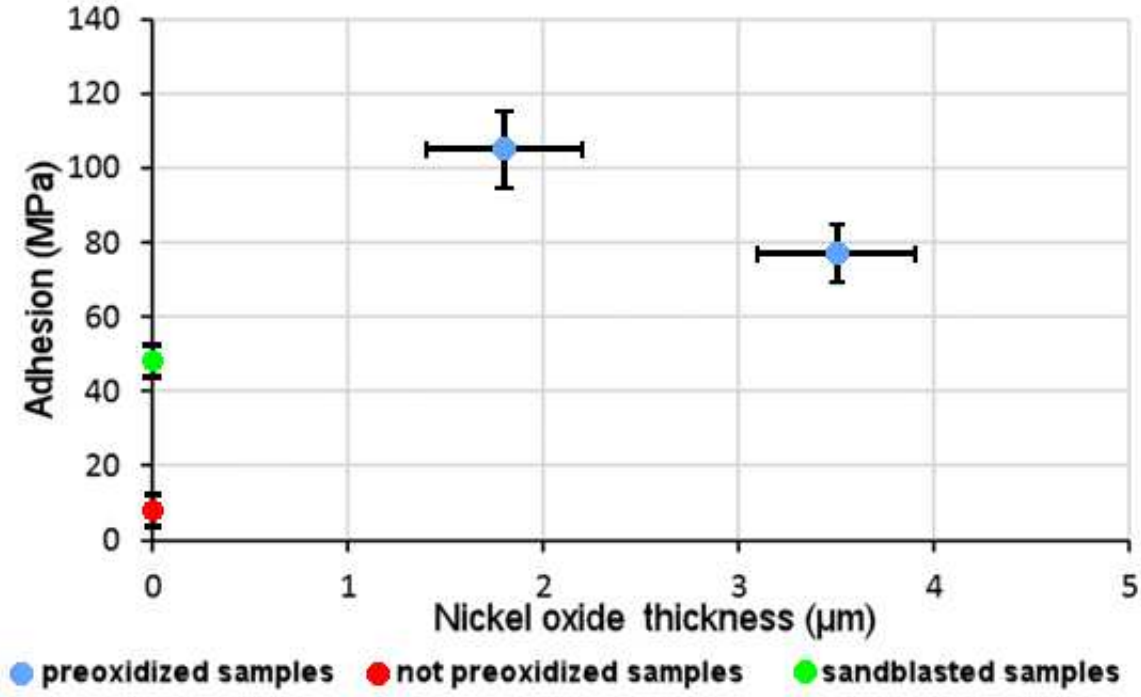
140
120
100
80
60
40
20
0
Adhesion (MPa)
0
1
2
3
4
5
Nickel oxide thickness (µm)
preoxidized samples
not preoxidized samples
sandblasted samples

Figure 14

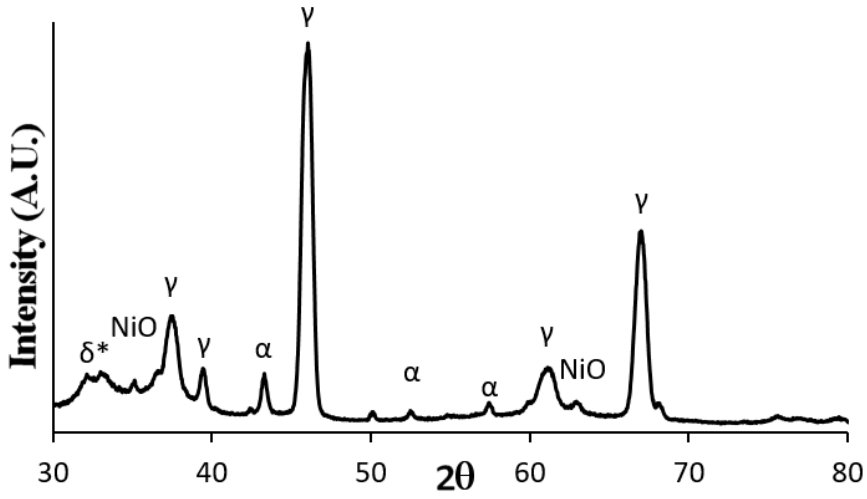

Figure 15

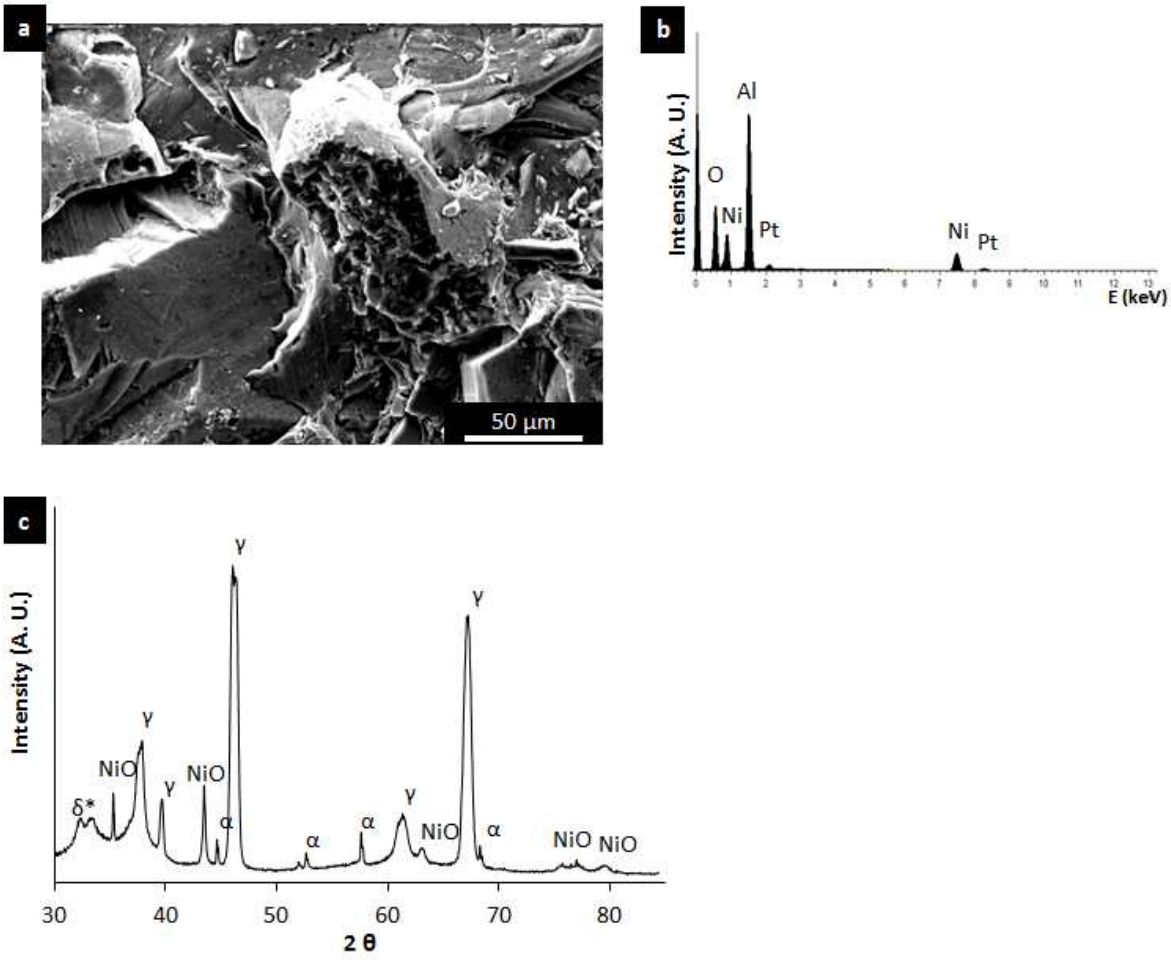
a
50 µm
b
Intensity (A. U.)
Al
O
Ni
Pt
Ni
Pt
E (keV)
c
Intensity (A. U.)
γ
γ
NiO
γ
NiO
δ*
α
α
α
γ
NiO
γ
α
NiO
NiO
30
40
50
60
70
80
2 θ

Figure 16

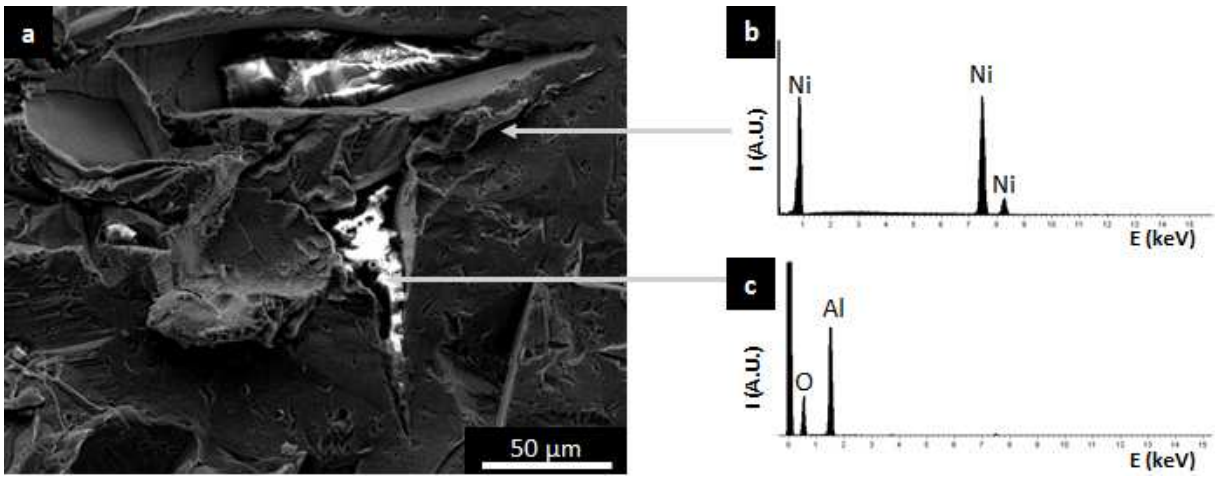

Figure 17

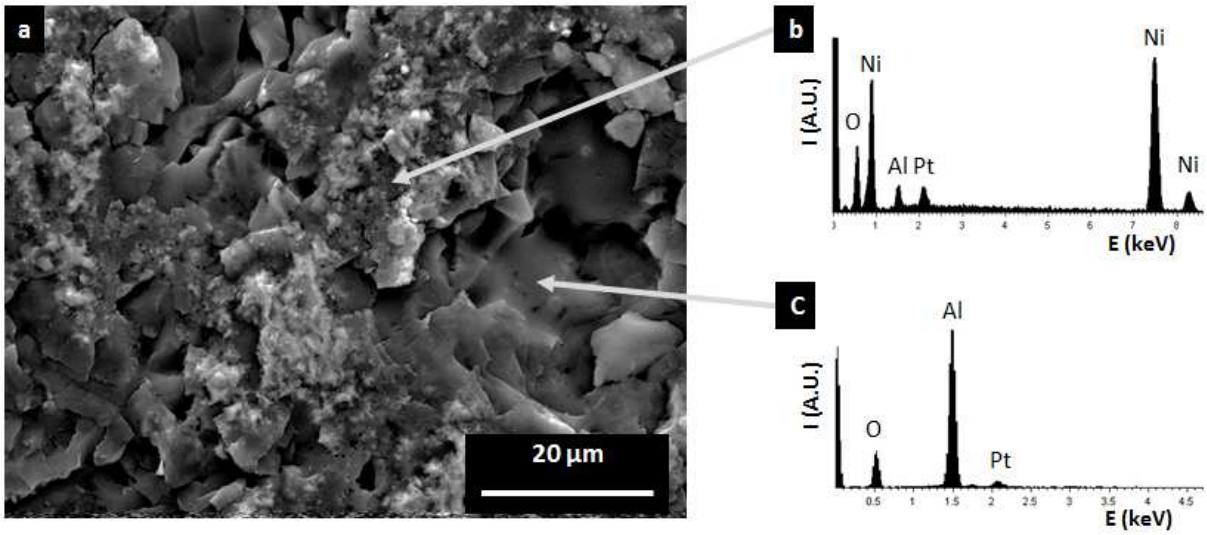

Figure 18

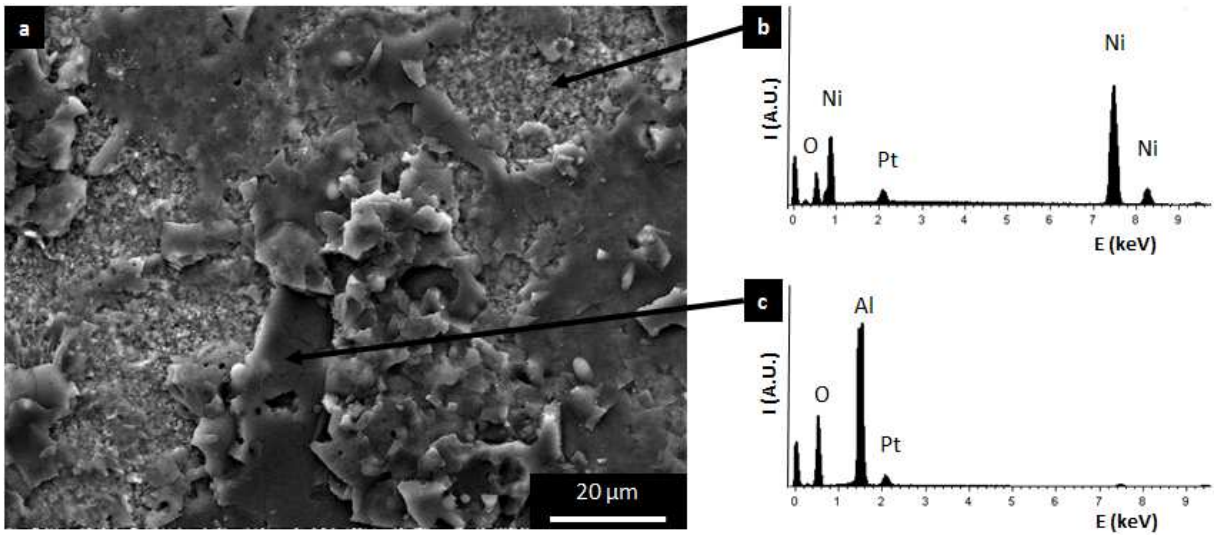

Figure 19